LARGE-EDDY SIMULATION OF ACCELERATING BOUNDARY LAYERS OVER ROUGH SURFACES

Junlin Yuan and Ugo Piomelli
Department of Mechanical and Materials Engineering
Queen's University
Kingston, ON, K7L 3N6, Canada
junlin.yuan@queensu.ca; ugo@me.queensu.ca

ABSTRACT

Large-eddy simulations (LES) are carried out to study the combined effects of roughness and pressure gradient in boundary layer flows, where the high acceleration facilitates flow reversion to the quasi-laminar state. First, validations of the immersed-boundary scheme and the LES resolution are carried out on rough-wall open-channel flows. Then the roughness model is applied to boundary layers subject to strong acceleration, leading to relaminarization and retransition. The roughness (represented by the roughness Reynolds number k^+) counteracts with the favourable pressure gradients (FPGs): while flow acceleration tends to stabilize the flow by significantly damping turbulent motions in the vertical and spanwise directions and produces one-dimensional turbulence after the high-acceleration region, the roughness elements increase the turbulent mixing in the wall layer, reducing the stability of the low-speed streaks, and leading to earlier retransition to turbulence.

INTRODUCTION

Turbulent boundary layers subject to a favourable pressure gradient induced by freestream acceleration are found in many engineering applications, including airfoils, turbine blades or ducts. If the acceleration is sufficiently large, turbulence production decreases, and the flow may revert to a laminar or quasi-laminar state. The acceleration can be characterized by the parameter

$$K = \frac{\nu}{U_\infty^2}\frac{dU_\infty}{dx}. \tag{1}$$

In sink flows (in which the acceleration acts for an infinite distance) Spalart (1986) showed that turbulence cannot be sustained if $K > K_{crit} \simeq 3\times10^{-6}$. In realistic spatially developing boundary layers, of course, the acceleration cannot be sustained for infinite distances, and complete relaminarization occurs rarely. The state of the flow is still significantly altered by strong acceleration, and even the mean velocity profile is changed, affecting, for example, separation. Once the cause of relaminarization is removed, the flow retransitions to turbulence in a process that may depend critically on the residual levels of turbulent fluctuations during the relaminarization.

Reviews of current knowledge can be found in several articles by Narasimha and Sreenivasan (Narasimha & Sreenivasan, 1973; Narasimha, 1985; Narasimha & Sreenivasan, 1979). Recent simulations of accelerating flows over smooth, flat plates (Piomelli *et al.*, 2000; De Prisco *et al.*, 2007) showed that the region of maximum acceleration is characterized by significant reorganization of the wall layer, with streaks that remain stable for very long distances. Frozen turbulence advected from upstream is still present and, once the acceleration ends, it triggers a bypass-like transition process. The outer layer is also affected: the turbulent structures become elongated and oriented in the streamwise direction due to the stretching caused by the freestream acceleration, and fewer outer-layer vortices survive, compared to a zero-pressure-gradient boundary layer.

It is well-known that roughness may significantly affect the characteristics of boundary layer flows (Raupach *et al.*, 1991; Jiménez, 2004) and promote transition to turbulence. Roughness, moreover, may occur in many of the applications in which favourable pressure gradients are also important (turbine blades, for instance). Therefore, a combined study of roughness and favourable pressure gradients on turbulent boundary layers may help the understanding of real-world boundary-layer flows in engineering applications. Experimental studies of the effects of both favourable pressure gradients and roughness were carried out by Cal *et al.* (2008, 2009); in these experiments the pressure gradients was below the threshold relaminarization, and the flow was quasi self-similar. They found competing effects of roughness and pressure gradients on the mean velocity, Reynolds stresses, and skin friction; these effects are reflected in the boundary layer parameter δ^*/δ.

In this study, we consider an accelerating boundary layer, with low Reynolds number at the inlet, subjected to a strong acceleration, with $K > K_{crit}$ for extended distances. We perform large-eddy simulations of the flow over both a smooth wall, and roughened walls with two equivalent sand-grain roughness heights $k = 0.2\delta_o^*$ and $0.4\delta_o^*$. In the following we present the problem formulation. We then discuss the numerical results, and finish with conclusions and recommendations

for future work.

PROBLEM FORMULATION

In LES, the filtered Navier-Stokes equations are solved. In incompressible flow, they are:

$$\frac{\partial \overline{u}_i}{\partial x_i} = 0; \quad \frac{\partial \overline{u}_i}{\partial t} + \frac{\partial \overline{u}_j \overline{u}_i}{\partial x_j} = -\frac{\partial \overline{p}}{\partial x_i} + \frac{1}{Re}\nabla^2 \overline{u}_i, \qquad (2)$$

where $Re = \delta_o^* U_{\infty,o}/\nu$ is the Reynolds number based on the freestream velocity and the displacement thickness at the inflow, $\overline{p}$ is the pressure divided by density, x_i are the Cartesian coordinates and $\overline{u}_i$ are the components of the velocity vector.

The simulations are performed using a well-validated staggered code, with second-order differences for all terms, semi-implicit time advancement, and MPI parallelization (Keating *et al.*, 2004). The unresolved SGS stresses are modeled using the Lagrangian Dynamic Eddy-Viscosity model (Meneveau *et al.*, 1996). We use periodic boundary conditions in the spanwise direction and a convective condition (Orlanski, 1976) for the outflow. At the inflow, the recycling/rescaling method by Lund *et al.* (1998) is used. At the freestream we use the same setup used in previous studies of this flow (Piomelli *et al.*, 2000; De Prisco *et al.*, 2007; Piomelli & Scalo, 2010): a profile of the streamwise time-averaged velocity $U_\infty(x)$ is assigned, and the mean freestream wall-normal velocity component, $V_\infty(x)$, is derived from mass conservation. Homogeneous Neumann conditions are applied to the fluctuating velocity components. The calculations are carried out at a Reynolds number $Re \approx 700$.

We used $1024 \times 170 \times 128$ grid points (in streamwise, vertical, and spanwise directions) to resolve a domain of dimensions $600\delta_o^* \times 20\delta_o^* \times 20\delta_o^*$. The grid is uniform in the spanwise directions, and stretched in the vertical directions, so that the first grid point is below $y^+ = 1$. In the streamwise direction, higher resolution is used in the regions with higher wall shear stress. The grid is fine enough to resolve adequately the roughness elements at the wall, which is verified by a grid refinement study performed for the low-roughness case.

Roughness elements are laid on the bottom wall, and the no-slip condition on the roughness surface is imposed by an immersed-boundary method (IBM). We use the virtual-sandpaper model proposed by Scotti (2006): the sand-grains are represented by uniformly distributed but randomly oriented ellipsoids of the same size (larger than the cell size) and the same shape. Only one parameter, the equivalent sand-roughness height k, is needed to describe the roughness geometry and distribution, with the semi-axes of the ellipsoids set to k, $1.4k$, and $2k$, and a separation of $2k$ between centers of neighboring ellipsoids in streamwise and spanwise directions. The roughness height k is chosen as $0.2\delta_o^*$ and $0.4\delta_o^*$ for the low- and high-roughness cases, which results in roughness Reynolds numbers within the transitionally rough regime in all cases (Table 1). Scotti (2006) proposed the use of an IBM based on the volume-of-fluid (VOF) approach: The fraction of the volume of each cell occupied by the fluid, ϕ, is calculated in pre-processing, and a force is imposed on the right-hand side of the momentum equation to reduce the velocity proportionally to the solid volume fraction in each cell.

Table 1. Parameters for simulations of FPG boundary layer flow over rough surfaces ($Re_{\delta^*} \approx 700$ at the inflow). The grid is stretched in x-direction, and uniform in z-direction.

k/δ_o^*	0.2	0.4
High acceleration:		
k^+	$7-23$	$16-61$
Δx^+	$20-40$	$20-66$
Δz^+	$6-17$	$6-24$
Low acceleration:		
k^+	$7-10$	$15-23$
Δx^+	$20-26$	$20-30$
Δz^+	$6-7.7$	$6-8.6$

Although the VOF method is only first-order accurate (Fadlun *et al.*, 2000), we consider it sufficient for this application, since the description of the boundary is only an approximation of a real sandpaper.

RESULTS

Since the IBM method had only been used in direct numerical simulations (DNS) of channel flow, we first verified that the decreased resolution of the LES still allowed the roughness effects to be simulated accurately. We performed simulations of open channel flow using the same parameters chosen by Scotti (2006), and obtained good agreement with the DNS. Piomelli & Scalo (2010) had performed DNS and LES of the accelerating boundary layer with the same parameters used here, and showed that the relaminarization process is captured correctly by an LES with the spacings used here, although the retransition occurs early, which is a common occurrence in under-resolved simulations (Ovchinnikov *et al.*, 2004).

As shown in Figure 1, K exceeds the critical value for relaminarization, $K_{crit} \simeq 3 \times 10^{-6}$, for extended lengths: around $54\delta_o^*$ (approximately $5\delta_o$, where δ_o is the boundary layer thickness at the inflow) in the low-acceleration case, and over $110\delta_o^*$ (approximately $10\delta_o$) for the high-acceleration one.

On the smooth plate C_f decreases in the high-acceleration region, indicating the occurrence of relaminarization; as the flow retransitions it increases again. The presence of roughness increases C_f, especially in the non-equilibrium region; comparison between the strong and weak acceleration cases shows that this effect is enhanced by acceleration. For the case with higher roughness, C_f never reduces below the value in the equilibrium region, indicating more vigorous turbulent transport throughout the acceleration region. The low-roughness case has a behaviour similar to that of the smooth plate, with significant decrease in the C_f (evidence of relaminarization) followed by earlier retransition (compared to the smooth case). Also, note that the difference between the LES and DNS, discussed by Piomelli & Scalo (2010), are confined to $x/\delta_o^* > 320$.

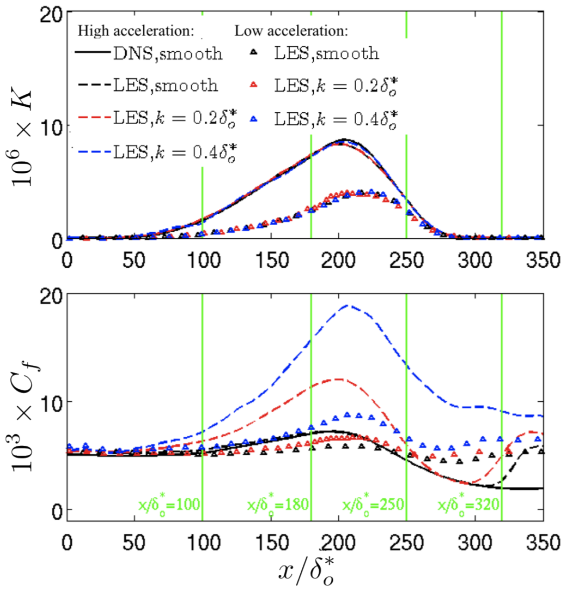

Figure 1. Streamwise development of the acceleration parameter (top), and skin-friction coefficient (bottom). Green lines indicate the locations where the mean velocity profiles are compared in Figure 2.

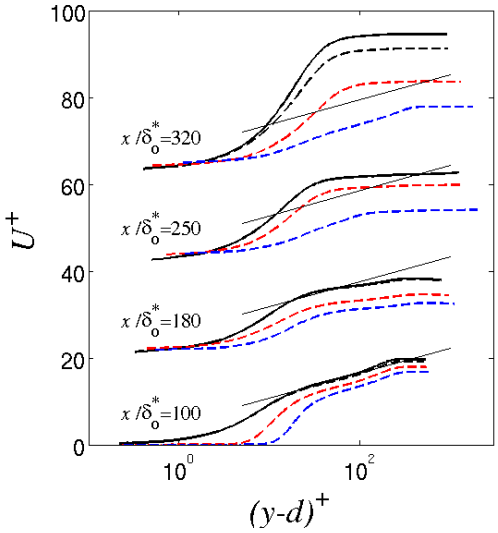

Figure 2. Mean velocity profiles in inner scaling for the strong-acceleration case. Streamwise stations are shown by green lines in Figure 1. ——— DNS (Piomelli & Scalo, 2010); - - - LES, smooth wall; - - - LES, $k=0.2\delta_o^*$; - - - LES, $k=0.4\delta_o^*$.

Figure 2 shows the mean velocity profiles, in wall units, at the four locations highlighted in Figure 1. The results are averaged both in the spanwise direction and in time (over an interval of $1200\delta_o^*/U_{\infty,o}$ time units). The virtual origin d is calculated as the vertical position where the mean drag force exerts on the surface, F, appears to act (Scotti, 2006):

$$d=\frac{\int_0^y \eta F(\eta)d\eta}{\int_0^y F(\eta)d\eta}, \tag{3}$$

The average value of d/k is very close to 0.8, the same as the value reported by Scotti (2006) for an open-channel flow with this roughness model. This value is not noticeably influenced by the freestream acceleration, probably because it is only determined by the distribution of drag force from the bottom wall to the tip of the roughness elements, which is not sensitive to flow acceleration.

In the retransition region the higher roughness results in a more rapid establishment of the logarithmic region; for the low-roughness case, on the other hand, the mean velocity profiles tend to collapse with the smooth-wall profiles in the region with decreased C_f; also the onset of retransition is similar for the smooth and low-roughness cases. Such a difference in flow reversion behaviours reveals competing effects between roughness and freestream acceleration: while the pressure gradient tends to relaminarize the flow, roughness counteracts this trend; for large roughness height, this effect will dominate the pressure gradient, and trigger earlier retransitions or eliminate the relaminarization all together. When the velocity profiles are plotted in outer scaling (not shown), we observe that all the curves collapse in the outer region, dominated by V_∞, which carries fluid from the irrotational region, resulting in a well-mixed outer layer with nearly zero velocity gradient.

The Reynolds stresses normalized by the local freestream velocity are shown in Figure 3 and 4 for the smooth and high-roughness cases, respectively. In the inner region, the vertical and spanwise components decrease faster than the streamwise one. A significant difference between rough and smooth cases is shown near the crest of the roughness elements in the region with a strong pressure gradient. Above the smooth wall, $\langle v'v'\rangle/U_\infty^2$ goes to zeros, producing zero shear stress, despite the non-zero streamwise Reynolds normal stress. Over the rough wall, on the other hand, the wakes of the roughness elements result in non-zero vertical fluctuations, and more significant Reynolds shear stresses; as a result, production is not shut down and the turbulence resumes its production cycles, leading to higher turbulent kinetic energy close to the wall after the recovery. In the low-roughness case (not shown here), the vertical disturbance induced by the roughness is not strong enough to trigger the recovery of production, and these locally active regions are immersed in the viscous sublayer. As a result, the flow behaves similarly to the smooth case.

To better understand the change in turbulent structures as a result of flow acceleration, we compare the streamwise component of the Reynolds stress anisotropy tensor

$$b_{ij}=\frac{\langle u_iu_j\rangle}{\langle u_ku_k\rangle}-\frac{\delta_{ij}}{3} \tag{4}$$

in Figure 5. For the smooth case inside the boundary layer, we observe a region with $b_{11}>0.6$, which indicates the estab-

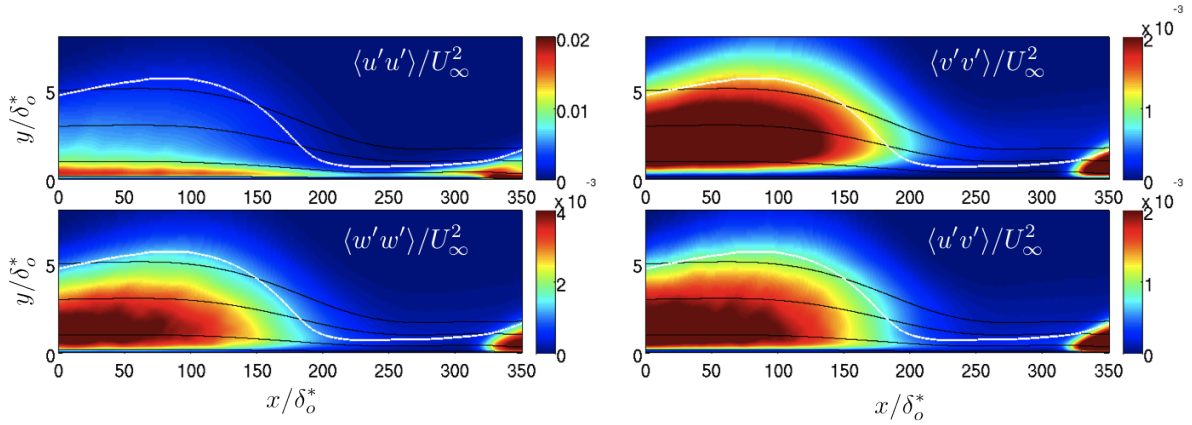

Figure 3. Reynolds stresses for accelerating flow over a smooth wall for the strong-acceleration case. The white line shows the boundary layer thickness, while black lines are mean-flow streamlines.

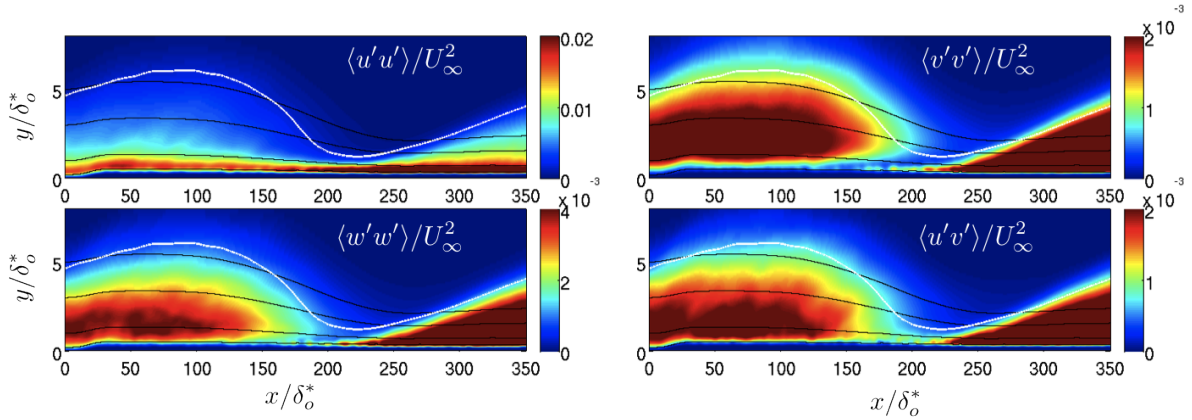

Figure 4. Reynolds stresses for accelerating flow over a rough wall (k/δ_o^*=0.4) for the strong-acceleration case. The white line shows the boundary layer thickness, while black lines are mean-flow streamlines.

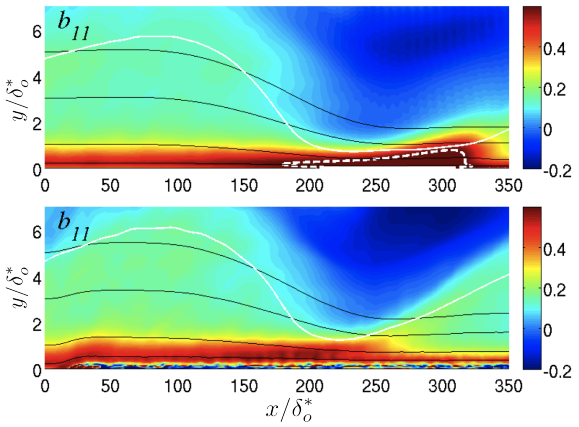

Figure 5. Streamwise Reynolds stress anisotropy b_{11} for the strong-acceleration case. The white line shows the boundary layer thickness, while black lines are mean-flow streamlines. The white dashed line encloses the region where $b_{11} \geq 0.6$.

lishment of quasi-1D turbulence; such region does not occur in the rough case.

The quasi-1D turbulence is due to a reorganization of the near-wall turbulence, which can be illustrated by instantaneous contours of the velocity fluctuations u' in a plane near the wall (Figure 6). When the wall is smooth we observe the well-known establishment of very elongated streaks, a symptom of the stabilization of the inner layer and the disruption of the burst cycle. When high roughness is present, the elongated streaky structures in the high-FPG region are disrupted by local disturbance and are never completely established. We also observe a smooth transition from the lower-*Re* turbulence structure in the initial part of the boundary layer to the smaller-scale turbulence in the high-*Re* region downstream due to higher U_∞.

The isosurfaces of the second invariant of the velocity gradient tensor

$$Q = -\frac{1}{2}\frac{\partial u_i}{\partial x_j}\frac{\partial u_j}{\partial x_i} \tag{5}$$

in Figure 7 show that the outer-layer structures are remarkably similar; near the wall, however, in the two rough-wall cases we observe a nearly uniform distribution of eddies in the region of roughness, generated by the wakes of the roughness

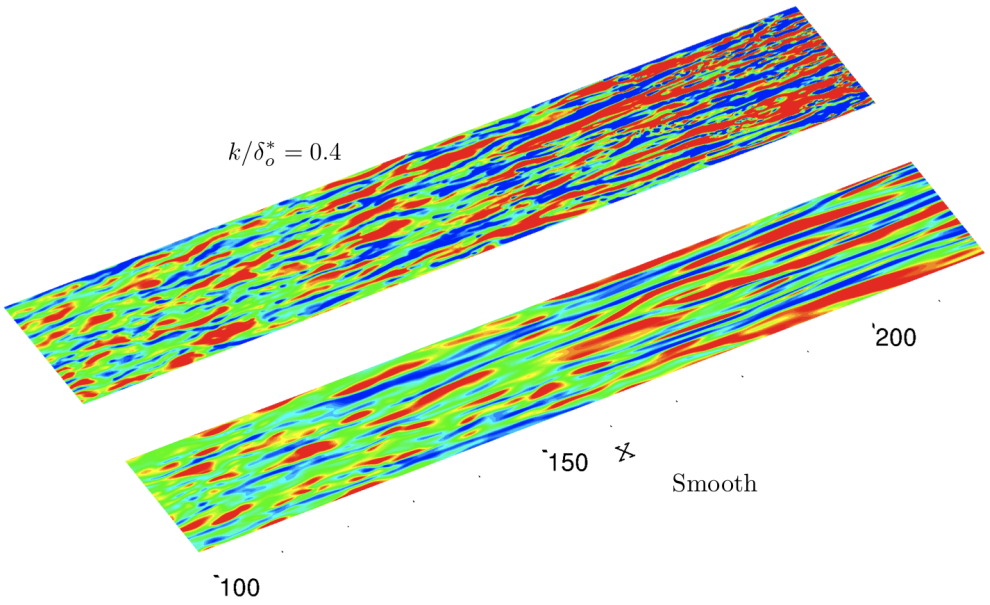

Figure 6. Contours of streamwise velocity fluctuations in the plane $y/\delta_o^* = 0.03$ for smooth-wall case (bottom) and $y/k = 1.5$ for rough-wall case with $k/\delta_o^* = 0.4$ (top), with the stronger acceleration.

elements, and essentially locked to the roughness element. These eddies increase mixing (as illustrated by the Reynolds stress contours), and play a role in the break-up of the streaks. However, when the roughness elements are small the disturbance they introduce does not penetrate far enough into the flow to break up the elongated streak, leading to a behaviour similar to the one on a smooth wall.

CONCLUSIONS

We have performed large-eddy simulations of the flow over smooth and rough-wall boundary layers subjected to favourable pressure gradients. Our results indicate that roughness plays a significant role in near-wall flow mixing, destabilizing the inner layer and reducing or eliminating relaminarization, by stimulating wall-normal velocity fluctuations close to the wall. Small-scale coherent structures are found to be generated in the wake of the roughness elements. For high k/δ_o^*, this prevents the flow from reorganizing under high freestream acceleration. However the combined effect of roughness and favourable pressure gradient depends on the relative significance of the two. The flow behaviour resembles a smooth-wall boundary layer in relaminarizing and retransitioning if the roughness height k/δ_o^* is small, although still in the transitionally-rough regime. Future works include studies on various roughness shapes, and quantification of bursts and streaks instability to further understand the competing mechanism between roughness and pressure gradient.

ACKNOWLEDGEMENTS

The authors thank the High Performance Computing Virtual Laboratory (HPCVL), Queen's University site, for the computational support. UP acknowledges the support of NSERC, under the Discovery Grant Program, and of the Canada Research Chairs Programme.

REFERENCES

Cal, R.B., Brzek, B., Johansson, T.G. & Castillo, L. 2008 Influence of the external conditions on transitionally rough favorable pressure gradient turbulent boundary layers. *J. Turbul.* **9** (38), 1–22.

Cal, R.B., Brzek, B., Johansson, T.G. & Castillo, L. 2009 The rough favourable pressure gradient turbulent boundary layer. *J. Fluid Mech.* **641**, 129–155.

De Prisco, G., Keating, A. & Piomelli, U. 2007 Large-eddy simulation of accelerating boundary layers. *AIAA Paper 2007-0725*.

Fadlun, E. A., Verzicco, R., Orlandi, P. & Mohd-Yusof, J. 2000 Combined immersed-boundary finite-difference methods for three-dimensional complex flow simulations. *J. Comput. Phys.* **161**, 35–60.

Jiménez, J. 2004 Turbulent flows over rough walls. *Annu. Rev. Fluid Mech.* **36**, 173–196.

Keating, A., Piomelli, U., Bremhorst, K. & Nešić, S. 2004 Large-eddy simulation of heat transfer downstream of a backward-facing step. *J. Turbul.* **5** (20), 1–27.

Lund, T. S., Wu, X. & Squires, K. D. 1998 Generation of inflow data for spatially-developing boundary layer simulations. *J. Comput. Phys.* **140**, 233–258.

Meneveau, C., Lund, T. S. & Cabot, W. H. 1996 A Lagrangian dynamic subgrid-scale model of turbulence. *J. Fluid Mech.* **319**, 353–385.

Narasimha, R. 1985 The laminar-turbulent transition zone in the boundary layer. *Prog. Aerosp. Sci.* **22**, 29–80.

Narasimha, R. & Sreenivasan, K. R. 1973 Relaminarization in highly accelerated turbulent boundary layers. *J. Fluid Mech.* **61**, 417–447.

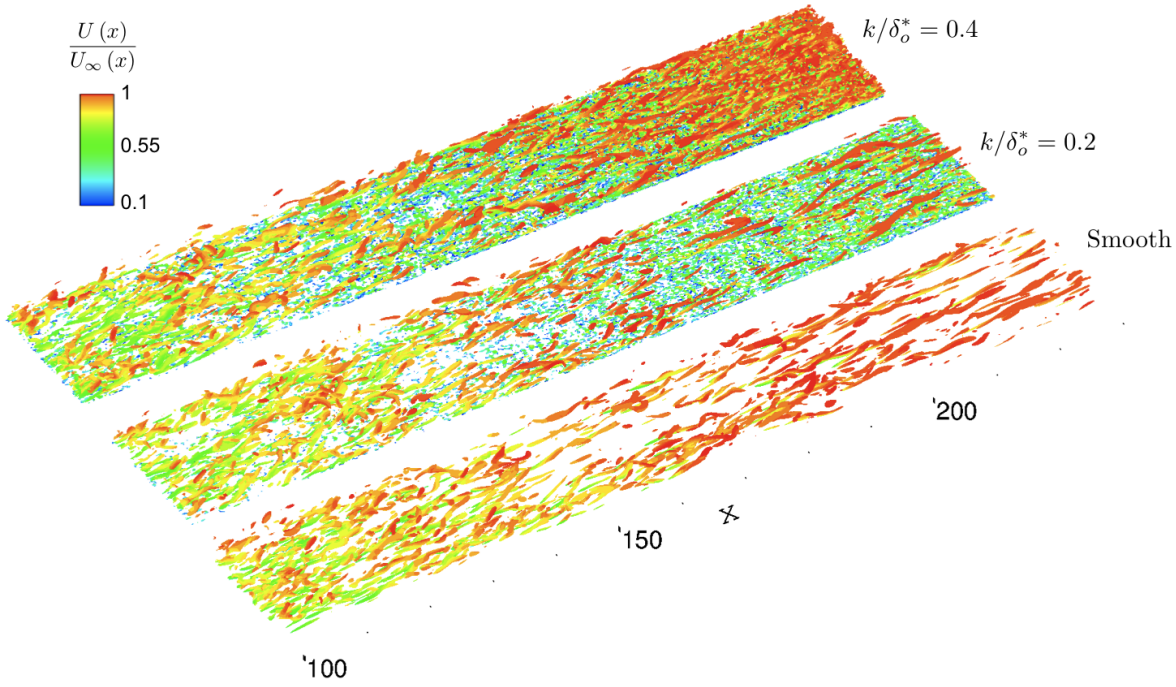

Figure 7. Isosurfaces of Q, coloured by U/U_∞. High roughness (top), low roughness (middle), and smooth case (bottom), with the stronger acceleration.

Narasimha, R. & Sreenivasan, K. R. 1979 Relaminarization of fluid flows. In *Adv. Applied Mech.*, , vol. 19, pp. 221–309. New York: Academic Press Professional, Inc.

Orlanski, I. 1976 A simple boundary condition for unbounded hyperbolic flows. *J. Comput. Phys.* **21**, 251–269.

Ovchinnikov, V., Piomelli, U. & Choudhari, M. M. 2004 Inflow conditions for numerical simulations of bypass transition. *AIAA Paper 2004-0491*.

Piomelli, U., Balaras, E. & Pascarelli, A. 2000 Turbulent structures in accelerating boundary layers. *J. Turbul.* **1** (1), 1–16.

Piomelli, U. & Scalo, C. 2010 Subgrid-scale modelling in relaminarizing flows. *Fluid Dyn. Res.* **42**, 045510.

Raupach, M. R., Antonia, R. A. & S., Rajagopalan 1991 Rough-wall boundary layers. *App. Mech Rev.* **44** (1), 1–25.

Scotti, A. 2006 Direct numerical simulation of turbulent channel flows with boundary roughened with virtual sandpaper. *Phys. Fluids* **18**, 031701.

Spalart, P.R. 1986 Numerical study of sink-flow boundary layers. *J. Fluid Mech.* **172**, 307–328.